Olmedo, A., Santiuste, C., & Barbero, E. (2014). An analytical model for the secondary bending prediction in single-lap composite bolted-joints. Composite Structures, 111, 354-361.

doi:https://doi.org/10.1016/j.compstruct.2014.01.015

An analytical model for the secondary bending prediction in single-lap composite bolted-joints

A. Olmedo, C. Santiuste and E. Barbero*

Department of Continuum Mechanic and Structural Analysis, University Carlos III of Madrid, Avda de la Universidad 30, 28911, Leganés, Madrid, Spain

*Corresponding author: Phone +34916249920, csantius@ing.uc3m.es

Abstract

The development of an enhanced analytical approach to predict the secondary bending of single-lap composite bolted joints is presented. The enhanced accounts for the estimation of secondary bending as a function of geometrical parameters, material properties, and stacking sequence. The model is validated through comparison of the predicted load-displacement curve with experimental tests and literature data. The model accuracy was validated for different values of bolt torque, friction coefficient, geometrical parameters, and material properties. The method has been also used in a parametric study to analyse the influence of the main joint parameters on the load-displacement curve. The model is a valuable preliminary design tool for analysing the influence of the joint parameters on the stiffness of single-lap composite joints including the effect of secondary bending.

1. INTRODUCTION

Composite materials combine fatigue and corrosion resistance, light weight and high specific stiffness and strength. These properties make composites suitable for a wide range of high responsibility applications in aeronautic industry. Mechanical joining is the most important method of assembling composite structural elements in the aerospace industry, due to its facility to assemble, disassemble and repair, and its tolerance to environmental effects [1]. However, fastener joints should be carefully designed due to the stress concentration at the surrounding of the hole. The stress concentration in composite laminates can be more critical than in metallic components [2,3]. The study of bolted joints in composite structural elements has received considerable attention in both the scientific literature and aeronautical standards [4-9].

The bolted joint performance depends on different parameters, mainly: joint geometry, plates and bolt materials, laminate layup, clearance, friction between different elements of the joint, temperature, load path, and bolt torque. The complex mechanical behaviour of composite bolted joints has been investigated by several researches by means of experimental studies, see for example [10-12]. However, due to the large range of parameters, the use of purely experimental techniques would be prohibitively expensive.

The development of theoretical reliable models is necessary to get a better understanding of all the aspect of the joint behaviour and to optimize the design of composite bolted joints.

Due to the complexity of composite bolted joints, several authors have proposed numerical models to analyse its mechanical behaviour but few studies have focused on the development of analytical models. The stiffness and the strength of bolted joints have been predicted with finite element models, showing good agreement with experimental data, [13-16]. Despite the accuracy of the finite element method to predict the failure of composite elements under different loading conditions [17,18], the development of simplify models can lead to a better understanding of the mechanical behaviour of composite bolted joints. Analytical models comprise the ability to explicitly describe the physical behaviour of bolted joints, and the possibility for conducting parametric studies.

The analyses of single-lap bolted joints have shown a non-uniform stress distribution throughout the thickness of composite plates in the surroundings of the hole due to the secondary bending produced by the eccentric load path [19-21]. This complex effect has been included in the formulation of simplified analytical models by mean of experimental coefficients [22-26].

Tate and Rosenfeld introduced a mass-spring model for double-lap joints made from isotropic materials [22]. Rosenfeld continued this work including experimental tests to validate the analytical model [23]. This simplified model was modified by Nelson et al. [24] to be applied to single-lap joints with anisotropic materials. To consider the influence of secondary bending on the joint stiffness, an experimental coefficient depending on the bolt configuration was included in the formulation. McCarthy et al. [25] modified the mass-spring model to add the effect of clearance. They predicted accurately the load-displacement curve and the load distribution obtained in experimental tests on single-column multi-bolt composite joints. McCarthy and Gray [26] improved the mass-spring model considering two steps in the load-displacement curve: the first dominated by friction forces and the second controlled by the contact stresses. The load-displacement curve was in agreement with experimental data. All these works considered an experimental coefficient to include the effect of secondary bending in the joint stiffness.

However, the results were validated with experimental data obtained from tests on single-column multi-bolt joints where the effect of secondary bending is limited. For an accurate prediction of the load-displacement curve in single-lap single-bolted joint configurations, secondary bending effect must be predicted with a more accurate method.

In this work, an analytical model to predict the stiffness of single-lap composite bolted joint is proposed. The model includes a predictive method to consider the effect of secondary bending as a function of geometrical parameters, material elastic properties, stacking sequence, and load path eccentricity. Experimental tests were developed to

validate the accuracy of the model results for different bolt torques. Also experimental data from literature were used to validate the analytical model analysing other materials and geometries. Moreover, a parametric study is include to investigate the influence of torque, friction coefficient, clearance, joint geometry, thickness, and material properties on the stiffness of composite bolted-joints.

2. MODEL DESCRIPTION

The present analytical model is an extension of the model proposed by McCarthy and Gray [26]. Fig. 1 shows the configuration of a single-lap single-bolt composite joint. To illustrate the mechanical behaviour of a highly torqued composite joint, Fig. 2 shows a typical load-displacement curve obtained in an experimental test. The curve can be divided in three regions. The first region corresponds to a quasi-linear behaviour produced by the load being reacted solely by static friction forces acting at the shear plane. With increasing loads, the static friction forces are overcome and the laminates slip relatively to each other with a uniform load. During this second region, the bolt-hole clearance is taken up and the bolt shank begins to contact the laminates. The third region starts when significant contact is established between bolt shank and hole surface, the bolt begins to transmit loads to the laminate and the joint stiffness increases significantly leading to a new quasi-linear region. The joint stiffness in the third region is strongly influenced by secondary bending phenomenon. The third region ends when the load reaches the bearing strength of the laminate, the objective of this work is to analyse the composite joint stiffness for loads below the bearing strength. This goal means an important contribution to understand the mechanical behaviour of composites joints and a necessary previous step to the development of future models including the prediction of bearing strength in single-lap composite joints.

The single-lap single-bolt composite joint may be represented by a system of masses and springs, as shown in Fig. 1. The joint load is applied at mass 3 and reacted at the clamped end of the joint. The stiffness of composite plate 1 under tensile loads is represented by K_{pl1}, and composite plate 2 by K_{pl2}. During the first region, the joint stiffness is dominated by the top branch, where $K_{sh\text{-}pl1}$ and $K_{sh\text{-}pl2}$ are the stiffnesses under shear load of composite plates 1 and 2 respectively. When the value of the load at top branch reaches the maximum value of the friction forces that the joint can transmit, a relative displacement between laminates is produced without increasing loads until the clearance is taken up. This phenomenon is represented by a friction element, F_{fricc}. When the contact between bolt shank and laminates is established, the joint stiffness is controlled by the bottom branch, where K_{bolt} includes the shear and bending stiffness of the bolt, the bearing stiffness of composite plates, and the secondary bending effect.

Considering that masses are free to move in the x-direction only, the system shown in Fig. 1 leads to a system of linear equations of the form:

$$[M]\{\ddot{x}\} + [K]\{x\} = \{F\} \quad (1)$$

For quasi-static loading, the accelerations can be neglected, leading to the next equation:

$$[K]\{x\} = \{F\} \quad (2)$$

Where the value of stiffness matrix [K] is modified for the different loading regions.

Free body diagrams for each mass during the first and third regions are shown in Figs. 3 and 4 respectively. Where c is the clearance between bolt diameter and hole, and u_f is the maximum displacement reached during the first region. The resulting linear equations during first and second regions are expressed in Eqs. (3) and (4) respectively. Calculation of the displacements is straightforward by pre-multiplying the load vector F by the inverse of stiffness matrix K.

$$\begin{bmatrix} K_{pl1} + K_{shear} & -K_{shear} & 0 \\ -K_{shear} & K_{shear} + K_{pl2} & -K_{pl2} \\ 0 & -K_{pl2} & K_{pl2} \end{bmatrix} \begin{bmatrix} x_1 \\ x_2 \\ x_3 \end{bmatrix} = \begin{bmatrix} 0 \\ 0 \\ F \end{bmatrix} \quad (3)$$

$$\begin{bmatrix} K_{pl1} + K_{bolt} & -K_{bolt} & 0 \\ -K_{bolt} & K_{bolt} + K_{pl2} & -K_{pl2} \\ 0 & -K_{pl2} & K_{pl2} \end{bmatrix} \begin{bmatrix} x_1 \\ x_2 \\ x_3 \end{bmatrix} = \begin{bmatrix} -K_{bolt} \cdot c - K_{bolt} \cdot u_f + F_{fricc} \\ K_{bolt} \cdot c + K_{bolt} \cdot u_f - F_{fricc} \\ F \end{bmatrix} \quad (4)$$

Calculations of spring stiffnesses.

The composite plate stiffness, in each plate i, can be found considering a composite laminate subjected to uniform tensile load:

$$K_{pli} = \frac{E_{Lci} \cdot W_{ci} \cdot t_{ci}}{p_{ci} - D/2} \quad (5)$$

Where E_{Lc} is the equivalent elasticity modulus in longitudinal direction calculated using the laminate theory. W_c and t_c are width and thickness of the composite plate respectively. p_c is the distance between the hole centre and the plate free end where load is applied, and D is the hole diameter.

The shear stiffness K_{shear} is found as the shear stiffnesses of the two composite plates in series.

$$K_{shear} = \left[\frac{1}{K_{sh-pl1}} + \frac{1}{K_{sh-pl2}}\right]^{-1} \quad (6)$$

Where the stiffnesses under shear load of composite plates 1 and 2, $K_{sh\text{-}pl1}$ and $K_{sh\text{-}pl2}$, are found considering the interlaminar stiffness of the laminate G_{xz}, the washer area in contact with the composite plate A_{wpli}, and the plate thickness t_{ci}. [26]

$$K_{sh-pli} = \frac{A_{Wpli} \cdot G_{xzi}}{t_{ci}} \quad (7)$$

The maximum value of friction forces that the joint can transmit, F_{fricc}, is obtained considering the friction coefficient and the normal force produced by the bolt torque.

$$F_{fricc} = \mu \cdot F_{torque} \quad (8)$$

Where μ is the friction coefficient, and the normal compressive force produced by the bolt torque can be found considering, Eq. (9) [27].

$$F_{torque} = \frac{\tau}{k \cdot D} \quad (9)$$

Where τ is the bolt torque and k is the torque coefficient usually taken as 0.2 [28].

The bolt stiffness has been obtained by previous researchers [22-24] considering the bolt shear stiffness, $K_{sh\text{-}b}$, the bolt bending stiffness, $K_{bend\text{-}b}$, the bearing stiffnesses of plates 1 and 2, $K_{be\text{-}pli}$, and an experimental coefficient, β, to include the secondary bending effect, Eq. (10).

$$K_{bolt} = \left[\frac{1}{K_{sh-b}} + \left[\frac{1}{K_{bend-b}} + \frac{1}{K_{be-pl1}} + \frac{1}{K_{be-pl2}}\right](1+3\beta)\right]^{-1} \quad (10)$$

The stiffnesses included in K_{bolt} can be found as follows:

$$K_{sh-b} = \frac{3G_b A_b}{2(t_{c1}+t_{c2})} \quad (11)$$

Where G_b is the bolt shear modulus, and A_b the bolt transverse section area.

$$K_{bend-b} = \frac{E_b t_{c1} t_{c2}}{2(t_{c1}+t_{c2})} \quad (12)$$

Where E_b is the bolt Young modulus.

$$K_{be-pl1} = t_{c1}\sqrt{E_{Lc1}E_{Tc1}} \quad (13)$$

$$K_{be-pl2} = t_{c2}\sqrt{E_{Lc2}E_{Tc2}} \quad (14)$$

Where E_{Tci} is the equivalent elasticity modulus of composite plate in transverse direction calculated using the laminate theory.

According to this formulation, the joint stiffness is strongly dependent on the secondary bending coefficient β, which was proposed as 0.15 for protruding heads joints by Nelson [24] and has been used by other authors [25,26]. However, the secondary bending depends on the joint geometrical parameters, material elastic properties, stacking sequence, and load path eccentricity. The main contribution of this work is the consideration of these parameters to estimate the secondary bending stiffness. Thus two springs are included in the model, $K_{\phi 1}$ and $K_{\phi 2}$, and the use of the secondary bending coefficient β, can be avoided Eq. (15).

$$K_{bolt} = \left[\frac{1}{K_{sh-b}} + \frac{1}{K_{bend-b}} + \frac{1}{K_{be-pl1}} + \frac{1}{K_{\phi 1}} + \frac{1}{K_{be-pl2}} + \frac{1}{K_{\phi 2}}\right]^{-1} \quad (15)$$

The present model considers the bolt shear stiffness, $K_{sh\text{-}b}$, the bolt bending stiffness, $K_{bend\text{-}b}$, the bearing stiffnesses of plates 1 and 2, $K_{be\text{-}pli}$, and the secondary bending stiffness of each plate, $K_{\phi i}$, in series. The secondary bending stiffness, $K_{\phi i}$, can be found considering that the joint transmit to the composite plates a transverse load P and a moment M_{ci}, see Fig. 5. The moments applied to the composite plates are in equilibrium with the moment produced by the eccentric load path, Eq. (16).

$$M_{c1} + M_{c2} = F \cdot t_m \quad (16)$$

Where t_m is the load path eccentricity estimated as the distance between the mid-plane of the composite plates.

The compatibility equations of rotations and transverse displacement where imposed using the laminate theory, Eqs. (17) and (18):

$$\phi_{c1} = \phi_{c2} = \frac{F\, t_m L_{efc1} L_{efc2}\left(L_{efc2}^3 E_{Fc1} I_{c1} + L_{efc1}^3 E_{Fc2} I_{c2}\right)}{L_{efc2}^4 E_{Fc1}^2 I_{c1}^2 + 2L_{efc1} L_{efc2} E_{Fc1} E_{Fc2} I_{c1} I_{c2}\left(2L_{efc1}^2 + 3L_{efc1} L_{efc2} + 2L_{efc2}^2\right) + L_{efc1}^4 E_{Fc2}^2 I_{c2}^2} \quad (17)$$

$$v_{c1} = v_{c2} = \frac{F\, t_m L_{efc1} L_{efc2}\left(L_{efc2}^2 E_{Fc1} I_{c1} + L_{efc1}^2 E_{Fc2} I_{c2}\right)}{2L_{efc2}^4 E_{Fc1}^2 I_{c1}^2 + 4L_{efc1} L_{efc2} E_{Fc1} E_{Fc2} I_{c1} I_{c2}\left(2L_{efc1}^2 + 3L_{efc1} L_{efc2} + 2L_{efc2}^2\right) + 2L_{efc1}^4 E_{Fc2}^2 I_{c2}^2} \quad (18)$$

Where, L_{efci}, is the distance between the hole surface and the plate free end where load is applied, E_{Fci} is the flexural modulus of the composite plate obtained with the laminate theory, and I_{ci} is the moment of inertia of the composite plate.

The longitudinal displacements were defined as a function of the rotations and plate thickness:

$$u_{ci} = \phi_{ci} \cdot \frac{t_{ci}}{2} \quad (19)$$

Then, the secondary bending stiffness, $K_{\phi i}$, can be defined as the ratio between the in-plane displacement and the load applied on the joint, F:

$$K_{\phi i} = \frac{F}{u_{ci}} \quad (20)$$

Thus the secondary bending stiffness for each composite plate yields:

$$K_{\phi 1} = \frac{2\left[L_{efc2}^4 E_{Fc1}^2 I_{c1}^2 + 2L_{efc1} L_{efc2} E_{Fc1} E_{Fc2} I_{c1} I_{c2}\left(2L_{efc1}^2 + 3L_{efc1} L_{efc2} + 2L_{efc2}^2\right) + L_{efc1}^4 E_{Fc2}^2 I_{c2}^2\right]}{t_{c1} t_m L_{efc1} L_{efc2}\left(L_{efc2}^3 E_{Fc1} I_{c1} + L_{efc1}^3 E_{Fc2} I_{c2}\right)} \quad (21)$$

$$K_{\phi 2} = \frac{2\left[L_{efc2}^4 E_{Fc1}^2 I_{c1}^2 + 2L_{efc1} L_{efc2} E_{Fc1} E_{Fc2} I_{c1} I_{c2}\left(2L_{efc1}^2 + 3L_{efc1} L_{efc2} + 2L_{efc2}^2\right) + L_{efc1}^4 E_{Fc2}^2 I_{c2}^2\right]}{t_{c2} t_m L_{efc1} L_{efc2}\left(L_{efc2}^3 E_{Fc1} I_{c1} + L_{efc1}^3 E_{Fc2} I_{c2}\right)} \quad (22)$$

3. VALIDATION

To validate the accuracy of the presented analytical model, experimental tests were conducted on single-lap single-bolted composite joints using a universal test machine Instron 8516. To guarantee quasi-static conditions a speed of 0.2 mm/min was applied. The composite parts were manufactured from carbon IM7 fibre and MTM-45-1 epoxy resin. Both laminates had quasi-isotropic lay-up with stacking sequence $[45/-45/0/90]_{3S}$. Its ply had a thickness of 0.125 mm, yielding a laminate thickness of 3 mm. The unidirectional lamina mechanical properties are listed in Table 1. The joint was assembled using a 4.8 mm diameter bolts made from aerospace grade titanium alloy 6Al4V, which properties can be found in table 1. The composite plates length and width were L_c=140 mm and W_c = 30 mm respectively; and the distance between the hole centre and the plate free end where load is applied was p_c = 135 mm.

To validate the accuracy of the analytical model two different values of bolt torque where applied, τ = 8 Nm and τ = 1 Nm. Figs. 6a and 6b show the load-displacement curves obtained in the experimental tests and the analytical model predictions. The solutions using the experimental coefficient β are also shown to illustrate the advantages of the present model. To validate the sensibility of the analytical model under other joints parameters, the model was also applied to reproduce the experimental data provided by the works of Ireman et al. [10], Fig. 6c, and Riccio and Marciano [11], Fig. 6d. Both studies considered a single-lap joint consisting of an 4 mm thick aluminium plate and a 4.8 mm thick laminate joined with a single bolt. The composite plates were made from a carbon/epoxy HTA 7/6376 laminate, and the aluminium plate from a 7475-T76 alloy. However, they considered different plate geometries, bolt diameters and torques. Ireman et al. used a $[\pm45/0/90]_{4S}$ stacking sequence and a 6 mm diameter bolt of titanium alloy 6Al 4V. The plates were 150 mm long and 36 mm wide, and the distance between the hole centre and the free end was 18 mm. The applied bolt torque was 1 Nm. Riccio and Marciano considered a $[0/\pm45/90]_{4S}$ stacking sequence and a 4.8 mm diameter bolt of titanium alloy 6Al 4V. The length and width of the plates were 150 mm and 28.8 mm respectively, the distance to the free end was 14.4 mm, and the bolt torque was 10 Nm.

Fig. 6 shows that the model predictions are in excellent agreement with experimental data. The model accuracy has been validated with different bolt torques, geometries and materials. The main advantage of the present model yields in the consideration of the secondary bending stiffness as a function of the plate geometry, material properties, stacking sequence, and load path eccentricity. The results showed an improvement in comparison with those obtained with a constant secondary bending coefficient. Moreover, the present model can explain the influence of the main joint parameters on the secondary bending and, as a consequence, on the stiffness of composite bolted-joints.

4. PARAMETRIC STUDY

A parametric study has been conducted to analyse the influence of the joint parameters on the stiffness of composite bolted-joints. The load-displacements curves obtained for different values of bolt torque, friction coefficient, clearance, and composite plate length are shown in Fig. 7.

The influence of bolt torque is shown in Fig. 7a, the values of bolt torque ranged from 1 Nm equivalent to tightening torque up to 8 Nm recommended by aeronautical standard ASTM D5961 [4] . The results showed that increasing values of bolt torque raised the maximum value of the friction forces that the joint can transmit, Eq. (8). Thus a higher load must be applied to produce a significant contact between the bolt shank and the hole surface, leading to a higher joint strength. Similar effect can be observed for increasing values of friction coefficient, Fig. 7b, because the maximum friction force that the joint can transmit is also increased. The friction coefficient ranged between 0.1 and 0.5 representing different surface roughness [16]. The influence of clearance between bolt and hole diameter is illustrated in Fig. 7c, considering values from 0 up to 200 μm according to the tolerance recommended in the ISO f7/H10 fitting. A high value of the clearance produces a great relative displacement between laminates leading to a significant reduction of the joint stiffness. These results are in agreement with the aeronautical standards recommendations to use high values of bolt torques and low clearances. The influence of composite plates length is shown in Fig. 7d. Increasing values of plate length lead to lower joint stiffness because the plate length affects to both the in-plane stiffness, Eq. (5), and secondary bending stiffness, Eqs. (20) and (21).

The load-displacement curves obtained for different composite plate widths, bolt diameters, thicknesses, and materials are shown in Fig. 8. Fig. 8a shows the influence of composite plate width. The plate width increases the joint stiffness only in the third region. The contribution of the width in the first region is negligible because the global stiffness is dominated by the shear forces applied in the region under the washer surface. The load-displacement curves obtained for diameter values between 4.4 mm and 5.2 mm are shown in Fig. 8b. These values of the diameter were chosen to guarantee a progressive failure of the joint due to bearing damage [6]. A reduction in the joint stiffness is only observed in the first region, where the stiffness is dominated by the friction forces transmitted by the washers. The joint stiffness is diminished because the effective area of the washers is reduced when the bolt diameter is increased.

Fig. 8c shows the load-displacement curves obtained for different thicknesses. The thickness was changed using different numbers of sublaminates in the quasi-isotropic stacking sequence $[45/-45/0/90]_{nS}$. In the first region, the slope of the force-displacement curve increases with decreasing values of the composite plate thickness due to an increment in the shear stiffness, Eq. (7). However, in the third region, the

slope is strongly increased with increasing thickness due to an increment in the secondary bending stiffness.

Five materials are compared in Fig. 8d: carbon/epoxi IM7/MTM-45-1, carbon/epoxi HTA7/6376 [16], carbon/epoxi T300/LTM45-EL [30], glass/epoxi Silenka 1200tex /DY063 [17], and Kevlar/epoxi K-285/ADR 240 [31]. The results showed a direct relationship between the material elastic properties and the joint stiffness. The three composite materials based on carbon fibres showed a higher stiffness than those composite made of glass or Kevlar fibres.

5. CONCLUSIONS

In this paper, a simple method for determining the effect of secondary bending on the stiffness of single-lap composite bolted joints has been presented. The present model calculates the secondary bending stiffness as a function of geometrical parameters, material elastic properties, stacking sequence, and load path eccentricity.

The method has been validated against experimental tests conducted with different bolt torques and experimental data found in scientific literature. The model proved to be accurate and robust being applied for different bolt torques, geometrical parameters, and material properties. The predictions of the load-displacement curve were in excellent agreement with experimental results. It has been shown that the estimation of secondary bending as a function of the joint parameters can improve the results obtained using experimental coefficients.

The method has been also used in a parametric study to illustrate the influence of the main joint parameters on the load-displacement curve. Both bolt torque and friction coefficient increased the force needed to create a significant contact between bolt shank and hole surface, leading to a higher joint strength. The clearance produces a relative displacement between laminates leading to a significant reduction of the joint stiffness. Increasing values of plate length lead to a lower joint stiffness. On the contrary, increasing values of plate width lead to a higher joint stiffness. If the bolt diameter is reduced, the joint stiffness increases only in the first region, where the stiffness is dominated by the friction forces. In the first region, the joint stiffness also increases with decreasing values of the plate thickness; however the stiffness of the third region is strongly reduced with deceasing thicknesses. The model has also shown a direct relationship between the material elastic properties and the joint stiffness.

The model is a valuable preliminary design tool for analysing the influence of the main joint parameters on the mechanical behaviour of single-lap composite joints including the effect of secondary bending. The results may be also useful for the development of future models to predict the bearing strength of single-lap composite bolted-joints considering non-uniform through-the-thickness distribution of stresses due to secondary bending.

ACKNOWLEDGMENTS

The authors are indebted for the financial support of this work to the Ministry of Science and Innovation of Spain (projects TRA2010_19573 and DPI2010-15123).

REFERENCES

[1] Camanho PP, Matthews FL. A progressive damage model for mechanically fastened joints in composite laminates. J Compos Mater 1999;33(24):2248-80.

[2] Olmedo A, Santiuste C, Barbero E. An analytical model for predicting the stiffness and strength of pinned-joint composite laminates. Compos Sci Technol 2014;90:67-73.

[3] Santiuste C, Olmedo A, Soldani X, Miguélez MH. Delamination prediction in orthogonal machining of carbon long fiber-reinforced polymer composites. J Reinf Plast Compos 2012;31(13):875-85.

[4] ASTM D5961. Standard test method for bearing response of polymer matrix composite laminates 2005.

[5] Tong L. Bearing failure of composite bolted joints with non-uniform bolt-to-washer clearance. Composites Part A 2000;31(6):609–15.

[6] Valenza A, Fiore V, Borsellino C, Calabrese L. Failure map of composite laminate mechanical joint. J Compos Mater 2007;41(8):951-64.

[7] Kapti S, Sayman O, Ozen M, Benli S. Experimental and numerical failure analysis of carbon/epoxy laminated composite joints under different conditions. Mater Des 2010;31(10):4933-42.

[8] Feo L, Marra G, Mosallam AS.Stress analysis of multi-bolted joints for FRP pultruded composite structures. Compos Struct 2012;94(12):3769-80.

[9] Atas A, Soutis C. Subcritical damage mechanisms of bolted joints in CFRP

composite laminates. Compos Part B:Eng 2013;54:20-7.

[10] Ireman T, Ranvik T, Eriksson I. On damage development in mechanically fastened composite laminates. Compos Struct 2000;49(2):151–71.

[11] Riccio A, Marciano L. Effects of geometrical and material features on damage onset and propagation in single-lap bolted composite joints under tensile load: Part I - Experimental studies. J Compos Mater 2005;39(23):2071-90.

[12] Sen F, Pakdil M, Sayman O, Benli S. Experimental failure analysis of mechanically fastened joints with clearance in composite laminates under preload. Mater Des 2008;29(6):1159-69.

[13] Xiao Y, Ishikawa T. Bearing strength and failure behaviour of bolted composite joints (part II: modelling and simulation). Compos Sci Technol 2005;65(7-8):1032–43.

[14] Riccio A. Effects of geometrical and material features on damage onset and propagation in single-lap bolted composite joints under tensile load: Part II - Numerical studies. J Compos Mater 2005;39(23):2091-112.

[15] Santiuste C, Barbero E, Miguelez MH. Computational analysis of temperature effect in composite bolted joints for aeronautical applications. J Reinf Plast Compos 2011;30(1):3-11.

[16] Olmedo A, Santiuste C. On the prediction of bolted single-lap composite joints. Compos Struct 2012;94(6); 2110-17.

[17] Santiuste C, Soldani X, Miguélez MH. Machining FEM model of long fiber composites for aeronautical components. Compos Struct 2010;92(3):691-8.

[18] Santiuste C, Sanchez-Saez S, Barbero E. A comparison of progressive-failure criteria in the prediction of the dynamic bending failure of composite laminated beams. Compos Struct 2010;92(10):2406-14.

[19] Ireman T. Three-dimensional stress analysis of bolted single-lap composite joints. Compos Struct 1998;43(3):195-216.

[20] Ekh J, Schön J. Effect of secondary bending on strength prediction of composite, single shear lap joints. Compos Sci Technol 2005;65(6):953-65.

[21] Egan B, McCarthy CT, McCarthy MA, Frizzell RF. Stress analysis of single-bolt, single-lap, countersunk composite joints with variable bolt-hole clearance. Compos Struct 2012;94(3):1038–51.

[22] Tate MB, Rosenfeld SJ. Preliminary investigation of the loads carried by individual bolts in bolted joints. NACA TN 1051. 1946.

[23] Rosenfeld SJ. Analytical and experimental investigation of bolted joints. NACA TN 1458. 1947.

[24] Nelson WD, Bunin BL, Hart-Smith LJ. Critical joints in large composite aircraft structure. NASA CR-3710. 1983.

[25] McCarthy MA. McCarthy CT, Padhi GS. A simple method for determining the effects of bolt–hole clearance on load distribution in single-column multi-bolt composite joints. Compos Struct 2006;73(1):78-87.

[26] McCarthy CT, Gray PJ. An analytical model for the prediction of load distribution in highly torqued multi-bolt composite joints. Compos Struct 2011;93(2):287-98.

[27] Collings TA. The strength of bolted joints in multi-directional cfrp laminates. Compos 1977;8(1):43-55.

[28] Mischke CR, Budynas RG. Shigley's Mechanical Engineering Design. McGraw-Hill, 2008.

[29] Ridgard C. Complex Structures for manned/unmanned aerial vehicles. Low Temp Composite Processing Mechanical Property Data. Air Force Research Laboratory. AFRL-RX-WP-TM-2008-4054. 2008.

[30] Feito N, López-Puente J, Santiuste C, Miguélez MH. Numerical prediction of delamination in CFRP drilling. Compos Struct 2014;108:677-83.

[31] Bhattacharyya D, Horrigan DPW. A study of hole drilling in Kevlar composites. Compos Sci Technol 1998;58(2):267-83.

TABLE CAPTION

Table 1. Mechanical properties of IM7/MTM-45-1 carbon/epoxy composite material and 6Al-4V titanium alloy. Data from experimental results and literature [29,19].

FIGURE CAPTION

Fig. 1. Geometry and mass-spring model of a single-lap composite bolted-joint.

Fig. 2. Typical force-displacement curve for a single-lap single bolt composite joint.

Fig. 3. Free body diagrams for each mass during the first region.

Fig. 4. Free body diagrams for each mass during the second region.

Fig. 5. Loading conditions applied to composite plates to estimate the secondary bending stiffness.

Fig. 6. Load-displacement curves. Comparison between analytical model and experimental results. a) Bolt torque = 8 Nm. b) Bolt torque = 1 Nm. c) Bolt torque = 1 Nm [10]. d) Bolt torque = 10 Nm [11].

Fig. 7. Load-displacement curves, parametric study: Influence of a) bolt torque, b) friction coefficient, c) clearance, d) composite plate length.

Fig. 8. Load-displacement curves, parametric study: Influence of a) composite plate width, b) bolt diameter, c) stacking sequence, d) materials.

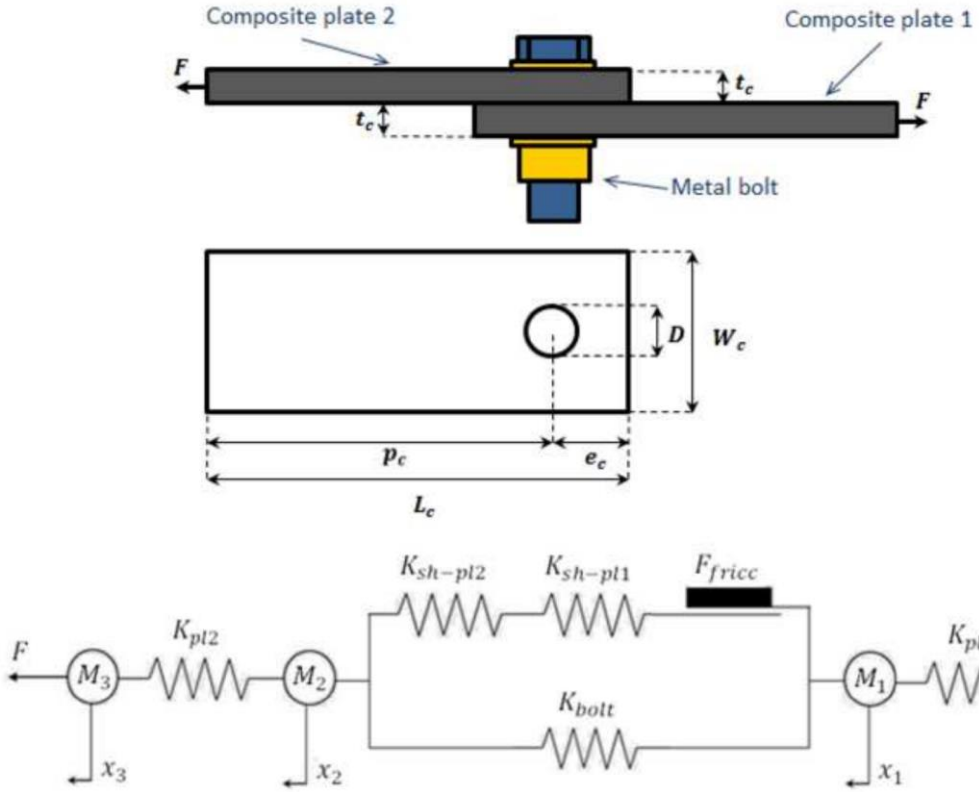
Composite plate 2
Composite plate 1
F
F
t_c
t_c
Metal bolt
D
W_c
p_c
e_c
L_c
K_{sh-pl2}
K_{sh-pl1}
F_{fricc}
K_{pl2}
K_{pl1}
F
M_3
M_2
M_1
K_{bolt}
x_3
x_2
x_1

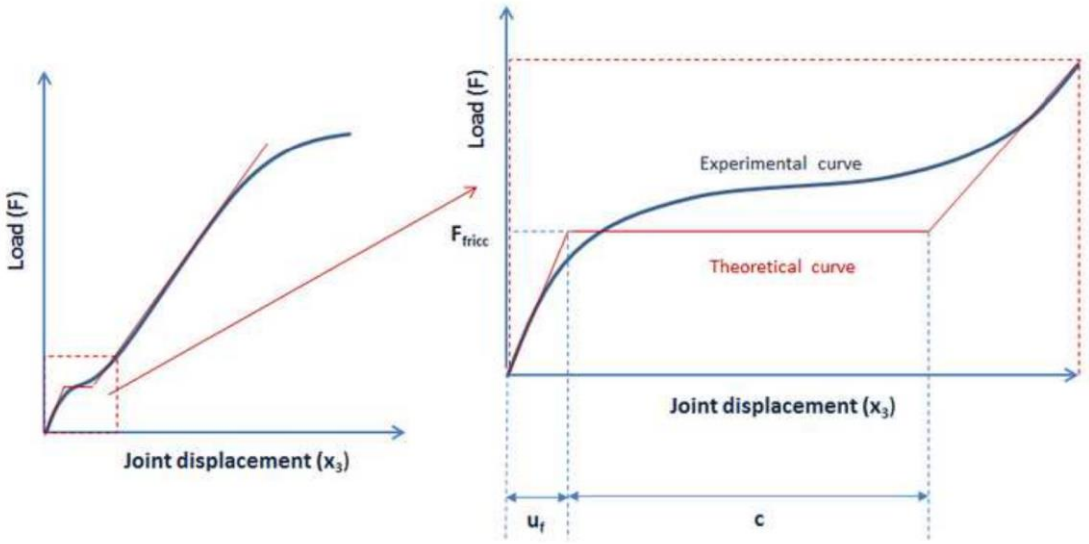
Load (F)
Joint displacement (x_3)
Load (F)
F_{tricc}
Experimental curve
Theoretical curve
Joint displacement (x_3)
u_f
c

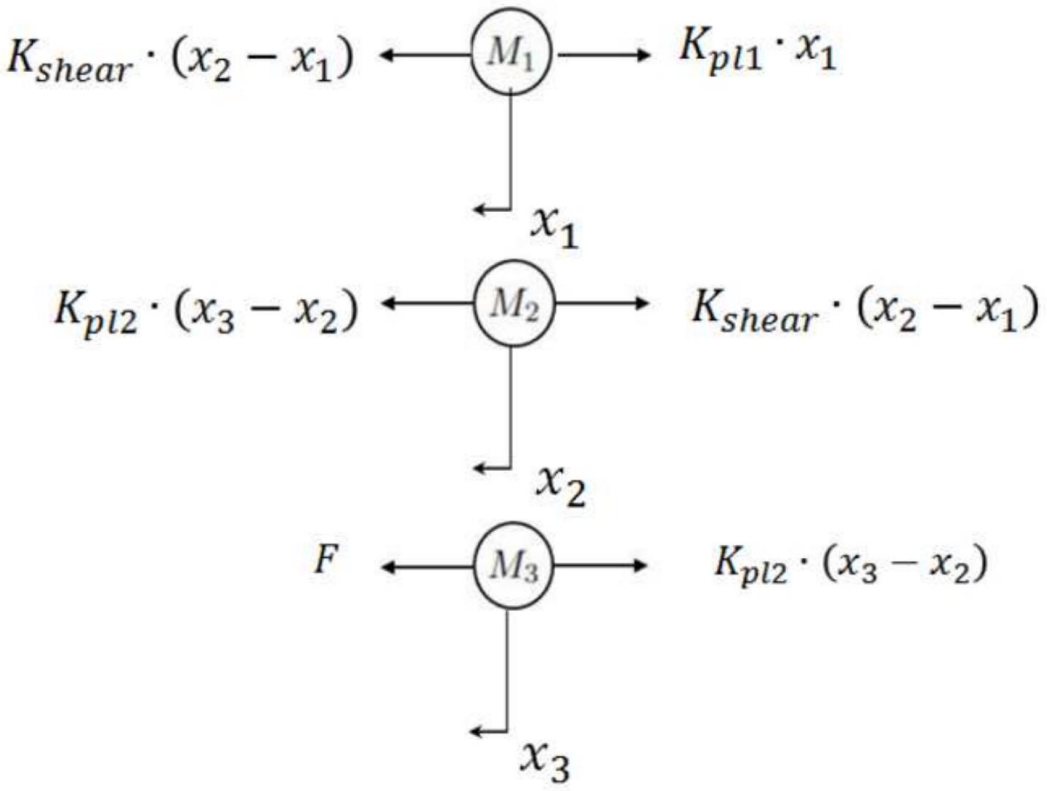
$K_{shear} \cdot (x_2 - x_1)$
M_1
$K_{pl1} \cdot x_1$
x_1
$K_{pl2} \cdot (x_3 - x_2)$
M_2
$K_{shear} \cdot (x_2 - x_1)$
x_2
F
M_3
$K_{pl2} \cdot (x_3 - x_2)$
x_3

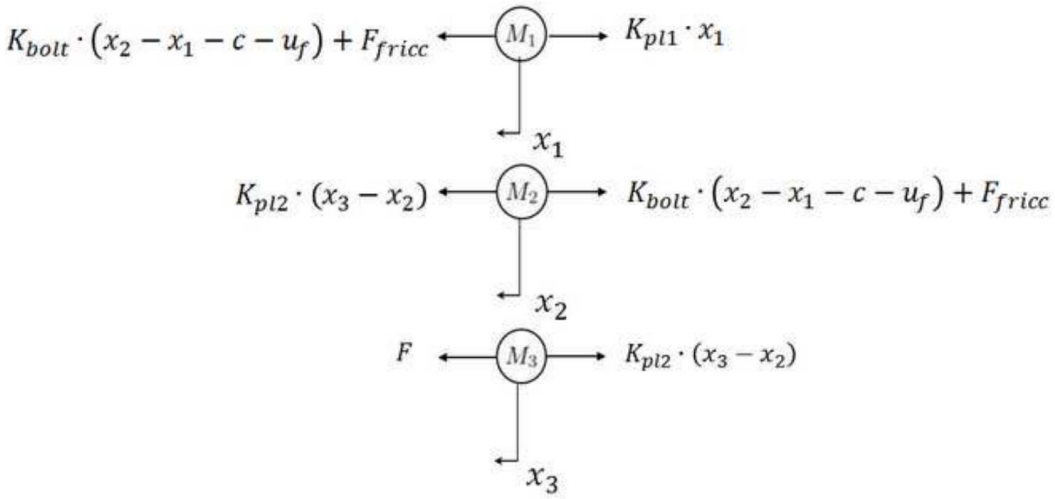
$K_{bolt} \cdot (x_2 - x_1 - c - u_f) + F_{fricc}$
M_1
$K_{pl1} \cdot x_1$
x_1
$K_{pl2} \cdot (x_3 - x_2)$
M_2
$K_{bolt} \cdot (x_2 - x_1 - c - u_f) + F_{fricc}$
x_2
F
M_3
$K_{pl2} \cdot (x_3 - x_2)$
x_3

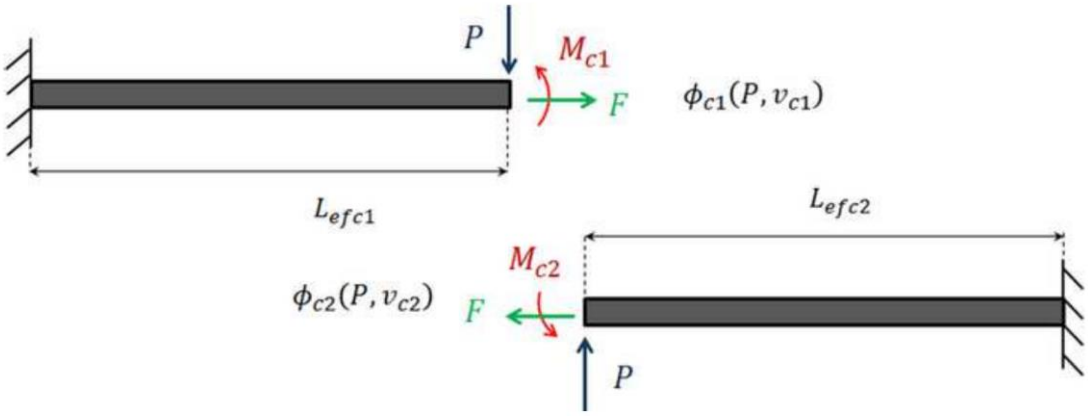
P
M_{c1}
F
$\phi_{c1}(P, v_{c1})$
L_{efc1}
L_{efc2}
M_{c2}
$\phi_{c2}(P, v_{c2})$
F
P

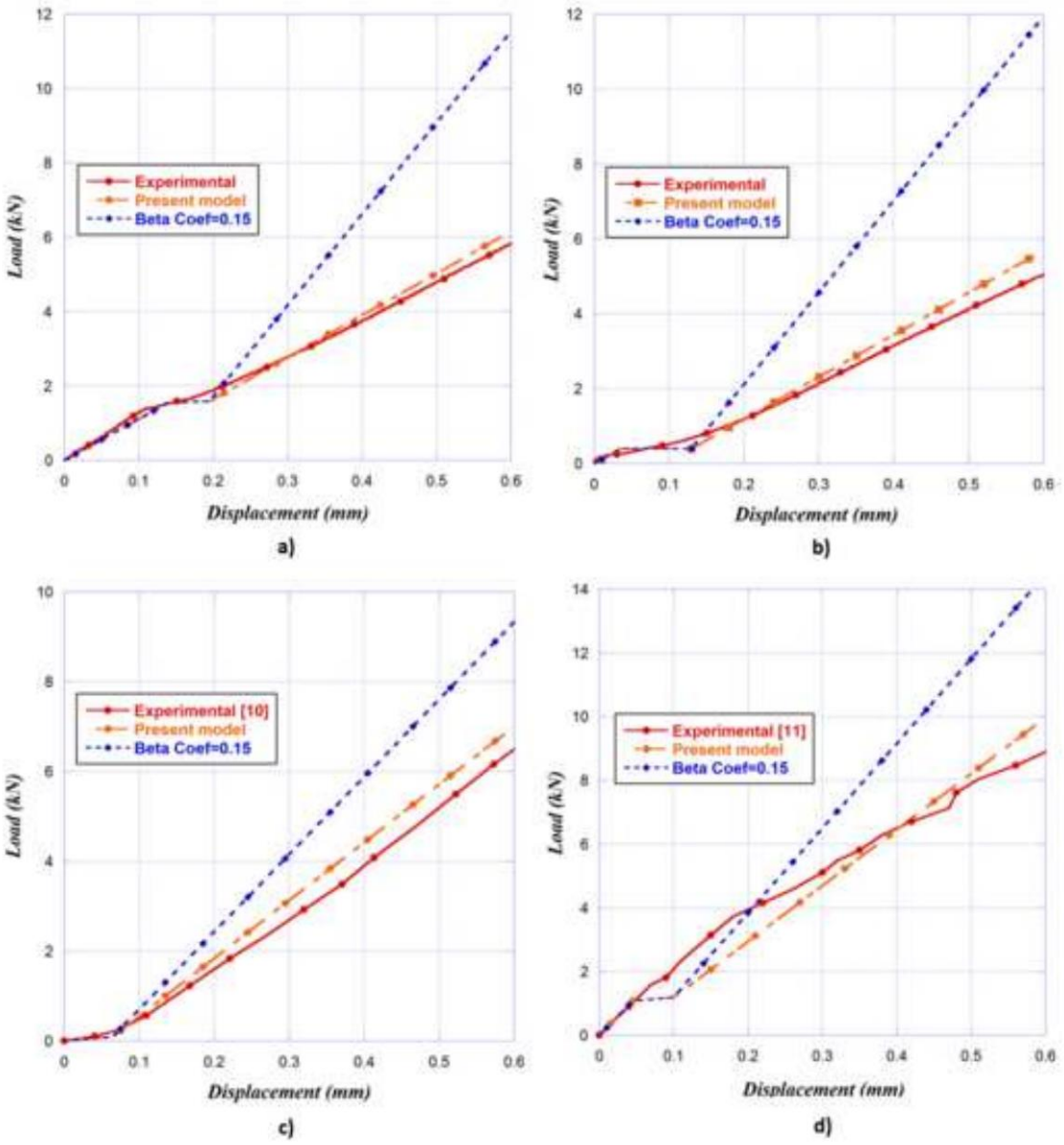
Experimental
Present model
Beta Coef=0.15
Load (kN)
Displacement (mm)
a)
b)
Experimental [10]
c)
Experimental [11]
d)

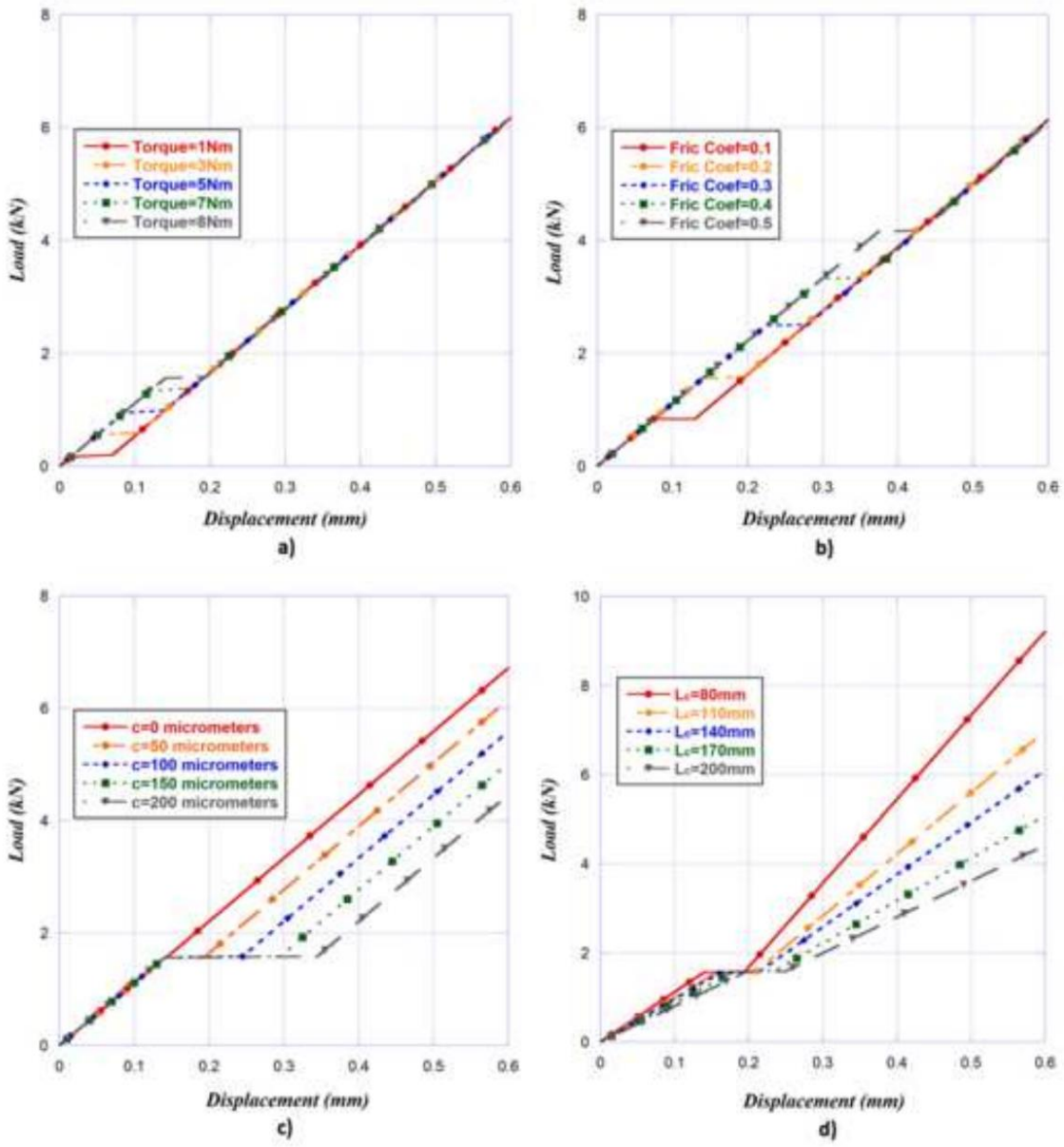
Torque=1Nm
Torque=3Nm
Torque=5Nm
Torque=7Nm
Torque=8Nm
Load (kN)
Displacement (mm)
a)
Fric Coef=0.1
Fric Coef=0.2
Fric Coef=0.3
Fric Coef=0.4
Fric Coef=0.5
Load (kN)
Displacement (mm)
b)
c=0 micrometers
c=50 micrometers
c=100 micrometers
c=150 micrometers
c=200 micrometers
Load (kN)
Displacement (mm)
c)
Lc=80mm
Lc=110mm
Lc=140mm
Lc=170mm
Lc=200mm
Load (kN)
Displacement (mm)
d)

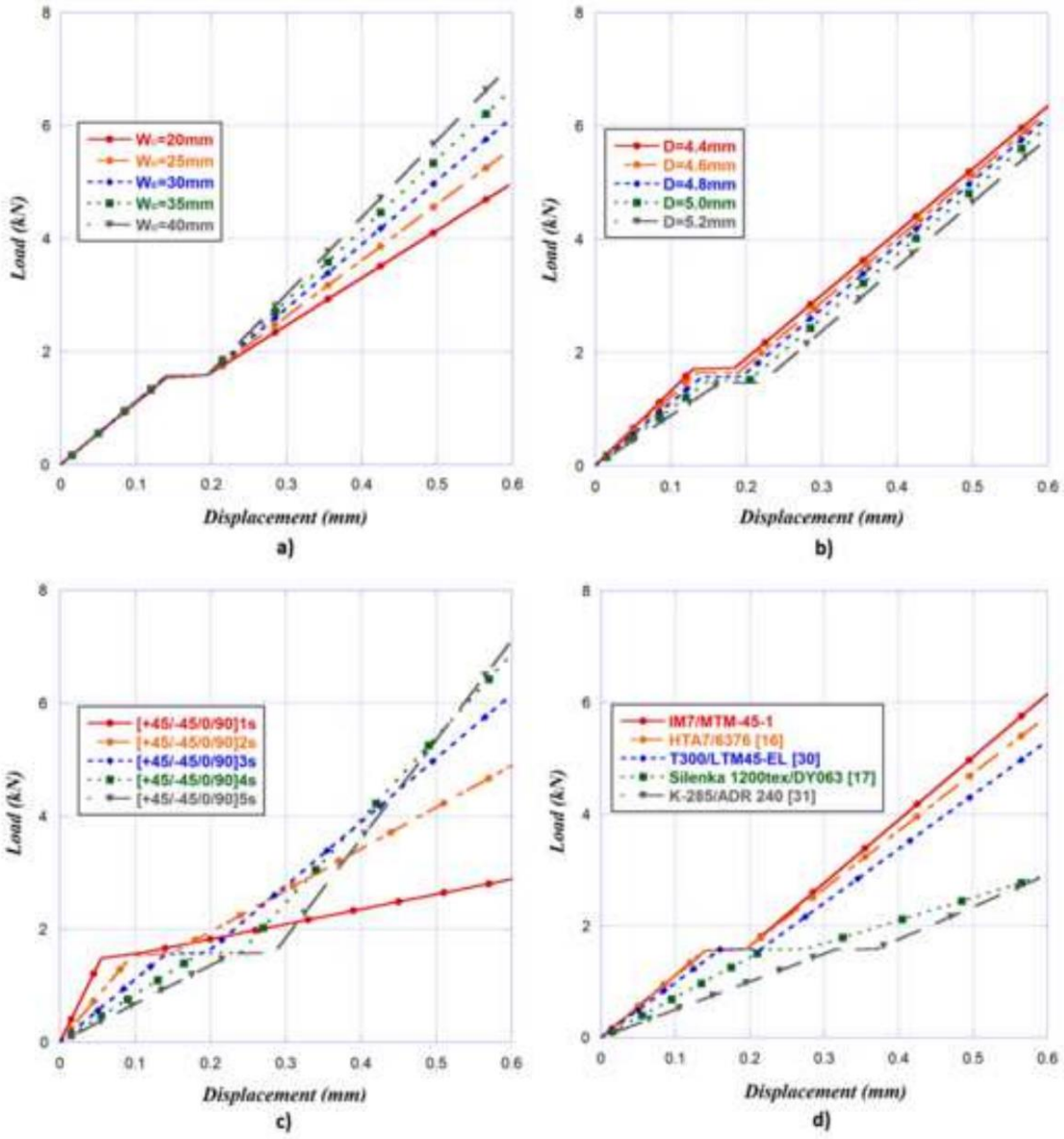
Load (kN)
Displacement (mm)
W=20mm
W=25mm
W=30mm
W=35mm
W=40mm
a)
D=4.4mm
D=4.6mm
D=4.8mm
D=5.0mm
D=5.2mm
b)
[+45/-45/0/90]1s
[+45/-45/0/90]2s
[+45/-45/0/90]3s
[+45/-45/0/90]4s
[+45/-45/0/90]5s
c)
IM7/MTM-45-1
HTA7/6376 [16]
T300/LTM45-EL [30]
Silenka 1200tex/DY063 [17]
K-285/ADR 240 [31]
d)